catalysts

MDPI

Article

K-Modulated Co Nanoparticles Trapped in La-Ga-O as Superior Catalysts for Higher Alcohols Synthesis from Syngas

Shaoxia Guo [1,2], Guilong Liu [3,4,*], Tong Han [5], Ziyang Zhang [1,2] and Yuan Liu [1,2,*]

1 Tianjin Key Laboratory of Applied Catalysis Science and Technology, School of Chemical Engineering, Tianjin University, Tianjin 300350, China; guosx@tju.edu.cn (S.G.); ziyang_zhang@tju.edu.cn (Z.Z.)
2 Collaborative Innovation Center of Chemical Science and Engineering (Tianjin), Tianjin 300072, China
3 College of Chemistry and Chemical Engineering, Luoyang Normal University, Luoyang 471934, China
4 Key Laboratory of Function-oriented Porous Materials of Henan Province, Luoyang Normal University, Luoyang 471934, China
5 Department of Material Science and Engineering, KTH Royal Institute of Technology, 11428 Stockholm, Sweden; tongh@kth.se
* Correspondence: glliu@tju.edu.cn (G.L.); yuanliu@tju.edu.cn (Y.L.); Tel.: +86-0379-68618321 (G.L.); +86-022-87401675 (Y.L.)

Received: 11 February 2019; Accepted: 22 February 2019; Published: 27 February 2019

Abstract: Owing to the outstanding catalytic performance for higher alcohol synthesis, Ga-Co catalysts have attracted much attention. In view of their unsatisfactory stability and alcohol selectivity, herein, K-modulated Co nanoparticles trapped in La-Ga-O catalysts were prepared by the reduction of $La_{1-x}K_xCo_{0.65}Ga_{0.35}O_3$ perovskite precursor. Benefiting from the atomic dispersion of all the elements in the precursor, during the reduction of $La_{1-x}K_xCo_{0.65}Ga_{0.35}O_3$, Co nanoparticles could be confined into the K-modified La-Ga-O composite oxides, and the confinement of La-Ga-O could improve the anti-sintering performance of Co nanoparticles. In addition, the addition of K modulated parts of La-Ga-O into La_2O_3, which ameliorated the anti-carbon deposition performance. Finally, the addition of K increased the dispersion of cobalt and provided more electron donors to metallic Co, resulting in a high activity and superior selectivity to higher alcohols. Benefiting from the above characteristics, the catalyst possesses excellent activity, good selectivity, and superior stability.

Keywords: perovskite-type oxide (PTO); cobalt; gallium; potassium; higher alcohols; syngas

1. Introduction

Due to their sufficient combustion and release of less harmful substances during combustion, higher alcohols with 2–6 carbon atoms are regarded as a kind of clean energy [1]. In addition, due to the high octane number, higher alcohols can also be used as a high-quality fuel additive. After separation, a series of basic chemicals with very high economic value, such as ethanol, propanol, and butanol, can be obtained [2–4]. Currently, ethanol is mainly produced by fermentation and ethylene hydration, while other alcohols are refined from petroleum. Obviously, in the long run, the above synthesis routes for higher alcohol would be restricted by increasingly depleted petroleum and food [5]. Recently, the synthesis of higher alcohols from syngas has attracted much attention, while this process is usually restricted by the low selectivity to higher alcohols and the poor stability of the catalyst.

Nowadays, four kinds of catalysts for higher alcohol synthesis (HAS) from syngas have been reported. Among them, the Rh-based catalysts show good activity and superior selectivity to ethanol, while the high price of Rh limits its industrial applications [6,7]. The harsh reaction conditions usually restrict large-scale applications for Mo-based catalysts [8,9]. For modified methanol synthesis catalysts,

the main product is still methanol [10,11]. Fortunately, modified Fischer–Tropsch catalysts, mainly the modified Co and modified Fe catalysts, exhibit good activity and high selectivity for HAS at milder reaction conditions. However, the modified Fe catalysts are more beneficial to the water gas shift reaction (WGSR), generating lots of CO_2; and the typical Cu modified Co catalysts usually show poor stability because of the phase separation of cobalt and copper [12–14]. Therefore, it has become an important issue for researchers to explore new catalysts for HAS from syngas with better catalytic performance.

Recently, Ga-modified Co catalysts were reported and showed excellent catalytic performance for higher alcohol synthesis [15–17]. He et al. prepared a series of Co-Ga catalysts by using Co-Ga-LDHs (layered double hydroxides) and found that Ga was beneficial to the non-dissociative adsorption of CO [15,16]. Gao et al. reported that gallium oxide can reduce the reduction degree of CoO and generate some Co^{2+} in the reduced catalysts, which act as non-dissociative CO adsorption sites for HAS, resulting in the high selectivity to alcohols for the Ga-Co/AC catalyst [17]. While the stability of Co-Ga catalysts should be further improved.

Here, considering the good activity and high selectivity on Co-Ga catalysts, K doped Co-Ga catalysts are explored by the reduction of $La_{1-x}K_xCo_{0.65}Ga_{0.35}O_3$. The results show that the addition of K modulates the composition of La-Ga-O, enhances the dispersion of Co, and adjusts the electronic structure of Co, and as a result the catalysts possess excellent catalytic performance. Typically, an outstanding selectivity of 43.6% to the higher alcohols, and a stable catalytic performance during the 200 h reaction can be obtained.

2. Results and Discussion

2.1. X-ray Powder Diffraction (XRPD)

The X-ray powder diffraction (XRPD) patterns of the three catalysts for LCG ($LaCo_{0.65}Ga_{0.35}O_3$) and LKCG-x ($La_{1-x}K_xCo_{0.65}Ga_{0.35}O_3$, x = 0.1 and 0.2, where x is the K content in perovskite) (see 3.2 catalysis synthesis) are shown in Figure 1a. The diffraction peaks at 2θ = 23.2, 33.3, 40.6, 47.4 and 58.8° are attributed to the characteristic diffraction peaks of perovskite-type oxide (PTO). For LKCG-0.1 catalyst, with the addition of K ions into LCG, the perovskite diffraction peaks move to lower 2θ values (seen from the illustration of Figure 1a), for that the ion radius of K^+ (0.155 nm) is larger than that of La^{3+} (0.136 nm) [18]. The existence of perovskite structure after calcination is beneficial to the interaction and the even dispersion of all the elements.

For the LKCG-0.2, a new Co_3O_4 diffraction peak in Figure 1a can be seen. Since the amount of K entering the perovskite is limited, when the K doping amount is more than 0.1, part of potassium cannot incorporate into the perovskite structure and cover the surface of the catalyst in the form of oxide [18]. The presence of K_2O disrupted the dispersion of elements in the catalyst precursor, resulting in the formation of Co_3O_4. It is worth noting that a part of $LaCo_yGa_{1-y}O_3$ and $La_{1-z}K_zCo_{1-m}Ga_mO_3$ should also exist accompanied by the formation of Co_3O_4.

Meanwhile, Ga-containing oxides among the three samples cannot be detected, indicating that Ga entered into the structure of perovskite. The uniformly dispersed Co and Ga ions in the LKCG-0.1 catalyst are advantageous for the synergism between them, favoring the catalytic performance.

The XRPD profiles of three catalysts reduced at 750 °C (see 3.4 Catalysts' Performance) are presented in Figure 1b. As for LCG, the perovskite structure disappears and transfers to Co and $La_4Ga_2O_9$. As for the reduction of LKCG-0.1, phases of La_2O_3, Co, $LaGaO_3$, and a small amount of $La_4Ga_2O_9$ can be observed. The existence of the characteristic diffraction peak of $LaGaO_3$ and La_2O_3 indicated that the adding of K weakened the interaction between lanthanum and gallium. In other words, the addition of K in the perovskite modulated the composition of La-Ga-O, resulting in the change of La-Ga-O from $La_4Ga_2O_9$ to $LaGaO_3$ and La_2O_3.

Based on the above discussion in Figure 1a, parts of K cannot be doped into perovskite, resulting co-exist of $LaCo_yGa_{1-y}O_3$ and $La_{1-z}K_zCo_{1-m}Ga_mO_3$ in LKCG-0.2. During reduction,

$La_{1-z}K_zCo_{1-m}Ga_mO_3$ would be reduced into $LaGaO_3$ while $LaCo_yGa_{1-y}O_3$ to $La_4Ga_2O_9$, as a result, the LKCG-0.2 are reduced to $Co/LaGaO_3$-$La_4Ga_2O_9$, as can be seen in Figure 1b.

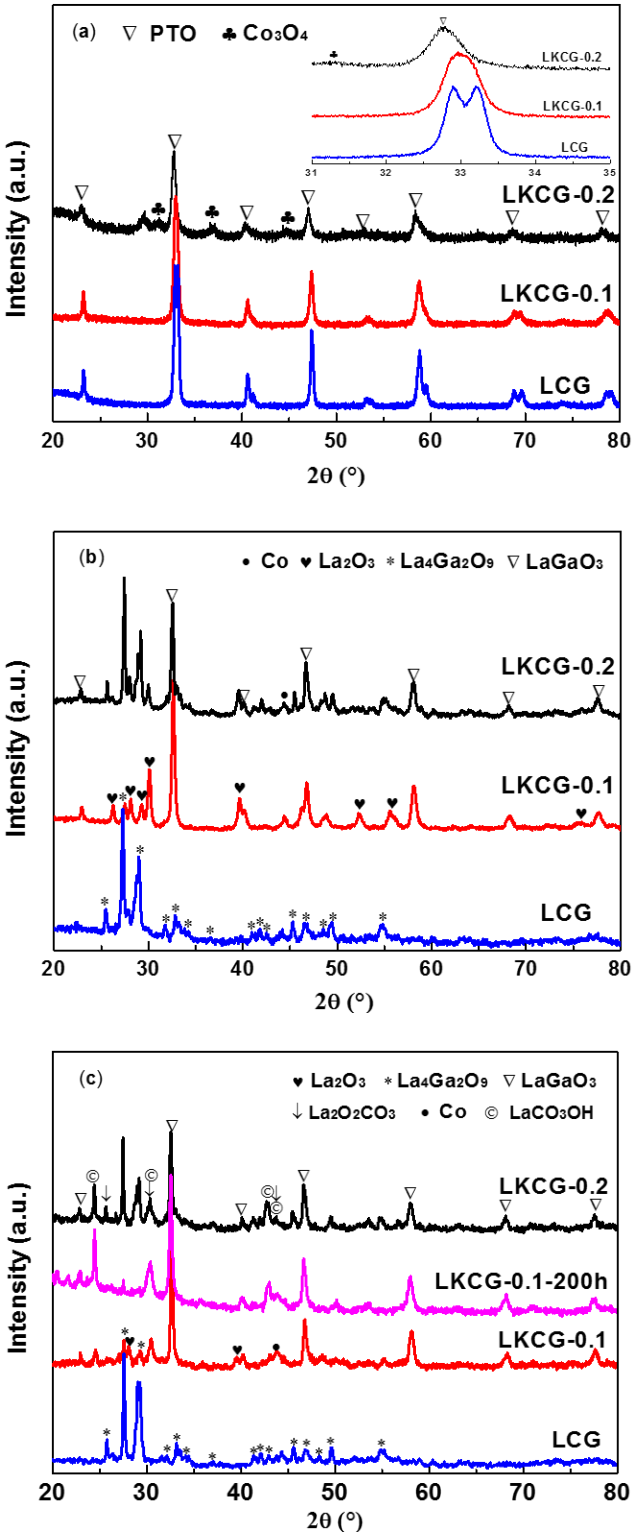

Figure 1. X-ray powder diffraction (XRPD) patterns of catalysts after (**a**) calcination, (**b**) reduction and (**c**) reaction.

Figure 1c shows the XRPD profiles of the three catalysts after reaction and LKCG-0.1 after 200 h reaction. After reaction, part of La_2O_3 transferred to $LaCO_3OH$ and $La_2O_2CO_3$, for that La_2O_3 and CO_2 can react to generate $La_2O_2CO_3$, and the further reaction between $La_2O_2CO_3$, H_2O and CO_2 can generate $LaCO_3OH$ [19,20]. Since XRPD in this work was carried out ex situ, the catalysts containing $La_2O_2CO_3$ could readily absorb H_2O and CO_2 in air, and then $LaCO_3OH$ formed. The co-existence of La_2O_3 and $La_2O_2CO_3$ in the catalysts after reaction illustrated the feasibility of reaction of $CO_2 + La_2O_3 \rightarrow La_2O_2CO_3 \xrightarrow{C} 2CO + La_2O_3$, which can help the catalysts eliminate carbon.

For the LCG catalyst after reaction, it should be noted that the catalyst was still $Co/La_4Ga_2O_9$, which is the same as that after reduction. $La_2O_2CO_3$ and La_2O_3 cannot be detected, indicating the above reaction of eliminating carbon deposition may be hard to occur due to a strong interaction existing between lanthanum and gallium.

It should be noted that no Co_2C was observed in all the used samples, suggesting that the existence of gallium can prevent the formation of Co_2C and stabilize the catalyst composition in the process of reaction. This is in accordance with the literature, which illustrated that the existence of gallium could improve the catalyst's stability [21].

2.2. Temperature-Programmed Reduction (TPR)

Figure 2 and Table 1 illustrates the temperature-programmed reduction (TPR) and the hydrogen consumptions values of LCG and LKCG-x (x = 0.1 and 0.2) catalysts. Seen from the Figure 2, all the three catalysts contain two major hydrogen-consuming peaks, one at 400–500 °C and the other at 600–800 °C. According to the literature, the H_2-consuming peak of $LaCoO_3$ at 500 °C can be attributed to $Co^{3+} \rightarrow Co^{2+}$, while that above 500 °C to $Co^{2+} \rightarrow Co^0$ [22–25]. Herein, seen from Table 1, the area ratio of the low temperature peak to the high temperature peak (T_L/T_H) is 1/2. Therefore, we believe that the peak of 400–500 °C in all the three catalysts is classified to $Co^{3+} \rightarrow Co^{2+}$, and the peak of 600–800 °C can be assigned to $Co^{2+} \rightarrow Co^0$. At the same time, the similar theoretical and experimental H_2-consumption also confirmed the attribution of the above reduction peak.

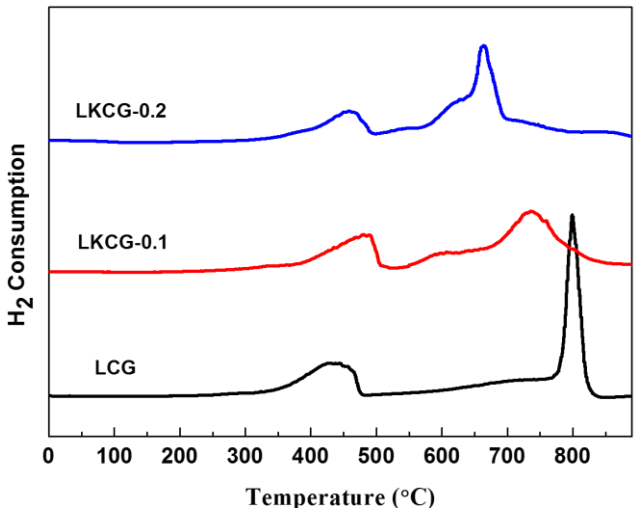

Figure 2. The temperature-programmed reduction (TPR) curves of catalysts after calcination.

Compared to the TPR results of $LaCoO_3$ in the literature, the H_2-consuming peak of $Co^{2+} \rightarrow Co^0$ migrates to higher temperatures in the LCG catalyst, suggesting that the existence of Ga in $LaCoO_3$ will restrain the conversion of Co^{2+} to Co^0 and a strong effect between Co and Ga exists for LCG [16].

Seen from Figure 2, with the addition of K ions in LCG, the H_2-consuming peaks at around 750 °C moved to lower temperature, illustrating the addition of K promotes the reduction of $Co^{2+} \rightarrow Co^0$. While for LKCG-0.2, a shoulder peak around 620 °C appeared. According to XRPD, the catalyst contains Co_3O_4. Therefore, this small shoulder can be attributed to the reduction of $Co^{2+} \rightarrow Co^0$ in

Co_3O_4. The presence of the small shoulder also confirms the XRPD results. For the other samples, no shoulders can be observed, which indicates that all the Co ions have entered into the crystal lattice of the perovskite.

Table 1. Theoretical and experimental H_2 consumption value of the LKCG-x (x = 0.1 and 0.2) and LCG catalysts.

Catalysts	Experimental Measure [a,b]		Theoretical Measure	
	T_L	T_H	$Co^{3+} \rightarrow Co^{2+}$	$Co^{2+} \rightarrow Co$
LCG	0.064	0.132	0.065	0.130
LKCG-0.1	0.067	0.133	0.068	0.135
LKCG-0.2	0.069	0.136	0.070	0.140

[a] Calculated from the TPR results. [b] The unit of H_2 consumption value is mmol H_2/50 mg. T_L and T_H represent low and high temperature, respectively.

2.3. N_2 Adsorption and Desorption Curves

Figure 3 and Table 2 show the N_2 physical adsorption curves and the physical properties of the investigated catalysts. Seen from the Figure 3, the curves are typical type II isotherms accompanying with a H_3 type hysteresis loop, which indicates that mesoporous exits in the catalysts. The presence of mesoporous can also be seen from the pore size distribution curves.

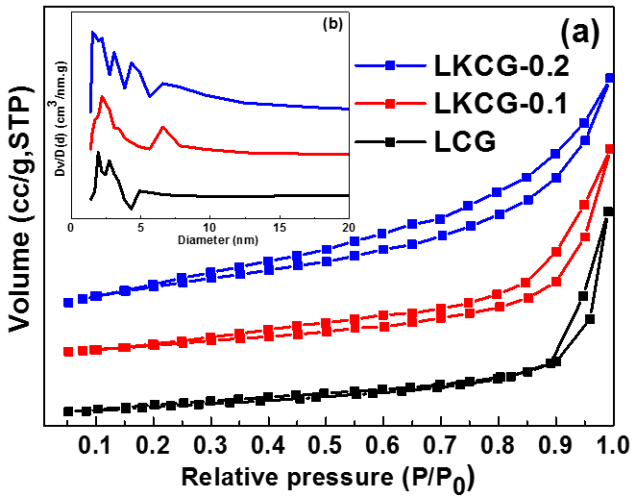

Figure 3. (**a**) The N_2 physical adsorption curves and (**b**) Barrett–Joyner–Halenda (BJH) pore size distribution of catalysts.

Table 2. The physical properties of all the investigated catalysts.

Catalysts	S_{BET} ($m^2\ g^{-1}$)	Pore Size (nm)	V_{BJH} ($cm^3\ g^{-1}$)	Crystal Size (nm) [a]		D_{Co} (%) [e]	d_{Co} (nm) [f]
				PTO	Co [b]		
LCG	8.6	14.9	0.03	17.4	15.9	7.3 [b] (6.1) [c]	13.2 [b] (15.7) [c]
LKCG-0.1	11.7	12.6	0.04	16.2	8.3	13.7 [b] (11.4) [c] (9.9) [d]	7.0 [b] (8.4) [c] (9.7) [d]
LKCG-0.2	15.0	9.8	0.04	13.4	7.4	15.5 [b] (12.6) [c]	6.2 [b] (7.6) [c]

[a] Calculated from X-ray diffraction results with the Scherrer equation. [b] The reduced catalysts. [c] The catalysts after reaction. [d] The 200 h stability test. [e] The degree of dispersion. [f] The crystal size calculated by hydrogen temperature-programmed desorption (H_2-TPD).

For LKCG-x (x = 0.1 and 0.2) catalysts, with the addition of K, the hysteresis loop increases and moves to lower P/P_0, illustrating the investigated catalysts have bigger BET surface area. The larger surface area results in the higher dispersion of metal cobalt nanoparticles (see in Table 2).

2.4. X-ray Photoelectron Spectroscopy (XPS)

Figure 4 and Table 3 summarized the binding energies (BEs) and the X-ray photoelectron spectroscopy (XPS) profiles of La 3d, Co 2p, and Ga 3d for the reduced LCG and LKCG-0.1 catalysts. All XPS profiles showed almost similar peak patterns except the different value of binding energies of each element. The binding energy of Co in the both samples is similar to that of metal cobalt, illustrating that Co exists in the form of Co^0 in the catalyst, which is the same as the XRPD results.

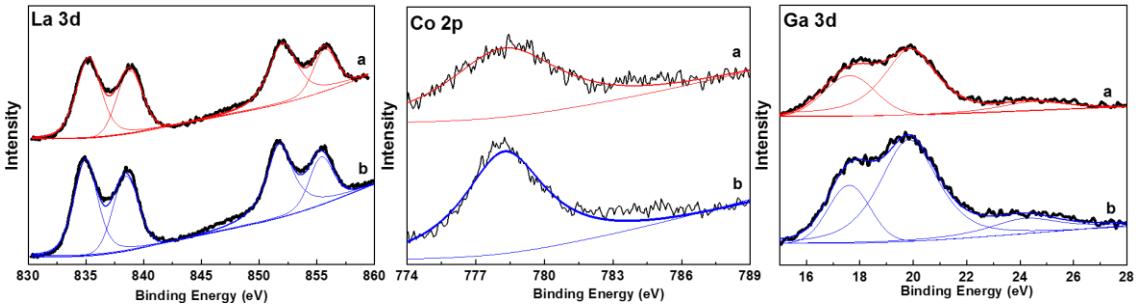

Figure 4. X-ray photoelectron spectroscopy (XPS) profiles of La 3d, Co 2p and Ga 3d of the reduced (**a**) LCG and (**b**) LKCG-0.1.

Table 3. The binding energies of the reduced LCG and LKCG-0.1 catalysts.

Catalysts	La $3d_{5/2}$		Co $2p_{3/2}$	Ga $3d_{5/2}$	
LCG	835.2	838.6	778.3	17.6	19.7
LKCG-0.1	834.9	838.4	778.1	17.7	19.8

According to the reported literature, the binding energies of La $3d_{5/2}$ are 834.4 and 837.8 eV for pure La_2O_3, 834.7 eV and 838.1 eV for $LaGaO_3$ [26–28]. Herein, the binding energies of La $3d_{5/2}$ for LCG are 835.2 eV and 838.6 eV, which is larger than that of pure La_2O_3 and $LaGaO_3$. The binding energies of Ga $3d_{5/2}$ are 17.6 and 19.7 eV, which is also a little larger than that of $LaGaO_3$ at 17.4 and 19.4 eV [28]. The binding energies of Co $2p_{3/2}$ is 778.3 eV, which is less than 778.5 eV for metal cobalt [29]. The higher binding energies of La $3d_{5/2}$ and Ga $3d_{5/2}$, and the lower binding energies of Co $2p_{3/2}$ illustrate that an interaction among La, Ga, and Co existed. At the same time, La and Ga could donate elector to Co.

Compared to the reduced LCG catalyst, it was found that the binding energy of La in LKCG-0.1 decreased, suggesting that the doping of K modulated the interaction between La and Ga, which agrees with the above XRPD results. In addition, the binding energy of Co is lower, which means that the K could donate electron to Co. The enhanced electron for Co is beneficial for the selectivity to higher alcohols.

2.5. Transmission Electron Microscopy (TEM)

Figure 5a–h shows the transmission electron microscopy (TEM) images, the line scans profiles, the energy dispersive spectrometer (EDS) mapping scans image, and the elements distribution of the reduced LKCG-0.1 catalyst. In Figure 5a, 5–11 nm Co nanoparticles are uniform dispersed in the reduced LKCG-0.1 catalyst even after 750 °C high temperature reduction. In Figure 5b, the lattice spacing of [112] and [011] planes for La_2O_3, [200] and [111] planes for metal Co, [220] planes for $La_4Ga_2O_9$ and $LaGaO_3$ can be clearly seen. That is to say, the composition of the reduced LKCG-0.1 catalyst is Co/La_2O_3-$La_4Ga_2O_9$-$LaGaO_3$, which is consistent with the XRPD. In addition, as seen from Figure 5b, the metal cobalt nanoparticles are encircled and located between La-Ga-O oxides. And this confinement effect result in the highly dispersion of Co nanoparticles in Figure 5a.

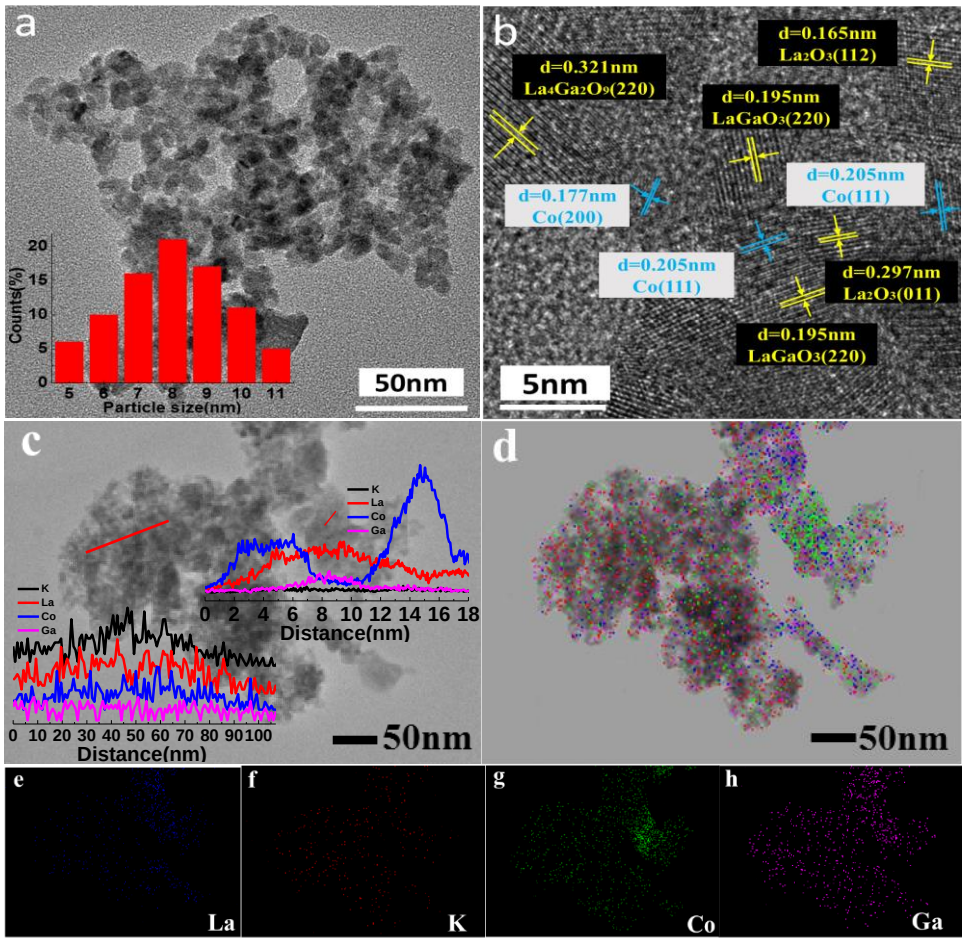

Figure 5. Transmission electron microscopy (TEM) images (**a**–**c**), line scanning profiles, energy dispersive spectrometer (EDS) mapping image (**d**), and the elements distribution of La (**e**), K (**f**), Co (**g**), and Ga (**h**) for the reduced LKCG-0.1.

Figure 5c–h exhibits the line scans profiles and the corresponding element distribution of the reduced LKCG-0.1 catalyst. The red lines represent the scanning routes in Figure 5c. Seen from the illustration in Figure 5c, the La and Ga have the same change trend, indicating the formation of La-Ga-O. In addition, there is no La and Ga where Co appears, illustrating metal cobalt nanoparticles are highly dispersed and located between the La-Ga-O oxides, which is in accordance with the XRPD and Figure 5b.

Figure 6a–h displays the TEM images, the line scanning profiles, the EDS mapping image, and the corresponding elements distribution of LKCG-0.1 after 200 h stability tests. As can be seen from Figure 6a, Co is still located between La-Ga-O oxide and the average crystal size of the Co nanoparticles is 9.5 nm, indicating that the sintering of the catalyst is not obvious, which is consistent with the results in Table 2. Seen from the Figure 6b, the lattice spacing of 0.205 and 0.177 nm are assigned to parameters of the [111] and [200] planes of Co; the lattice spacing of 0.228 nm, 0.276 nm, 0.306 nm and 0.294 nm corresponds to the [012], [200], [023], and [103] planes for La_2O_3, $LaGaO_3$, $La_4Ga_2O_9$ and $La_2O_2CO_3$, respectively. That is to say, the component of the LKCG-0.1 catalyst after 200 h reaction is Co/La_2O_3-$La_4Ga_2O_9$-$LaGaO_3$-$La_2O_2CO_3$, which is in accordance with the XRPD results.

2.6. CO Hydrogenation Performance

Table 4 lists the catalytic performance of all the investigated catalysts. The carbon monoxide hydrogenation performance of the different molar ratio of Co/Ga for $LaCo_yGa_{1-y}O_3$ catalyst were

explored in our lab, and the results revealed the optimum molar ratio is 0.65/0.35 [30]. Therefore, the molar ratio of Co/Ga of all the investigated samples was fixed at 0.65/0.35.

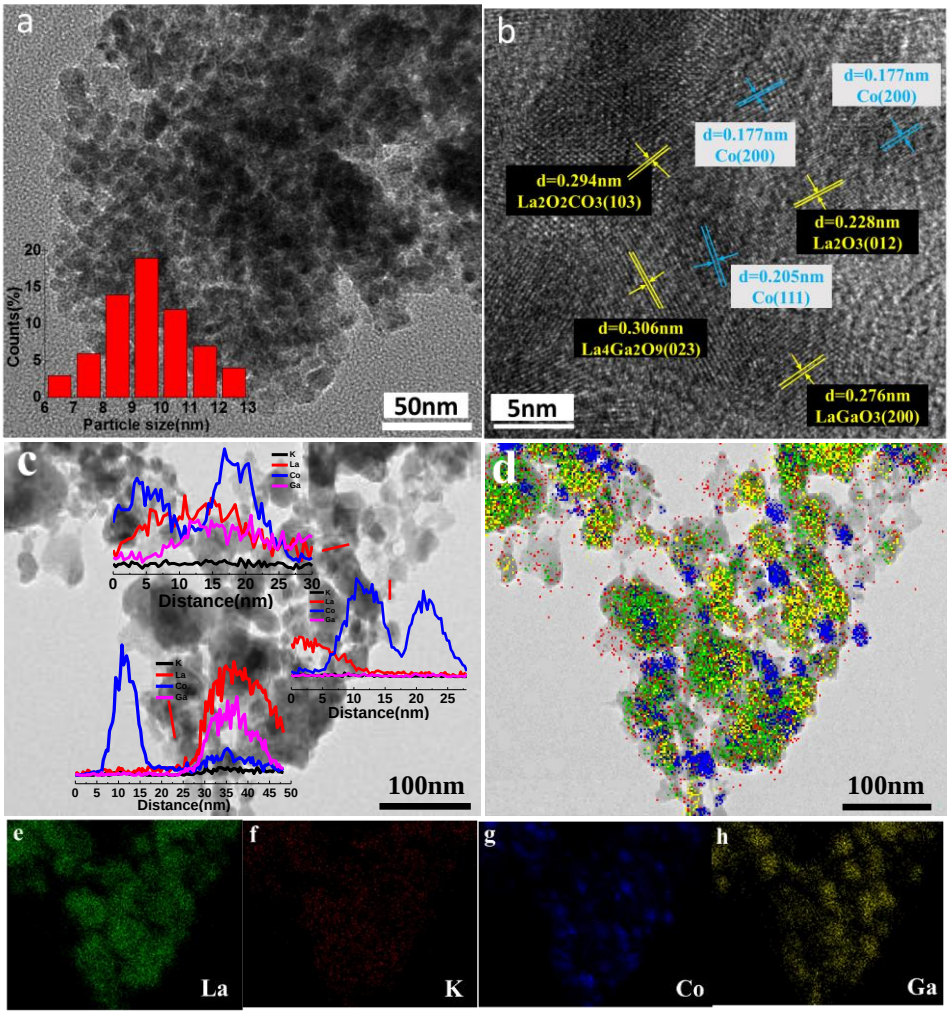

Figure 6. TEM images (**a**–**c**), line scanning profiles, EDS mapping image (**d**), and the elements distribution of La (**e**), K (**f**), Co (**g**), and Ga (**h**) for LKCG-0.1 after 200 h stability tests.

Table 4. CO hydrogenation performance of the investigated catalysts.

Catalysts	X_{co} [a] (%)	S_{co_2} [b] (%)	S_{ROH} [c] (%)	Selectivity to Hydrocarbon (%)				Distribution of Alcohols (%)			
				C_1	C_2	C_3	C_{4+}	C_1	C_2	C_3	C_{4+}
LCG	4.1	1.6	27.2	45.1	10.5	10.8	4.9	36.3	45.2	1.6	16.9
LKCG-0.1	13.2	5.8	43.6	24.7	9.2	11.9	4.8	30.9	58.1	3.2	7.8
LKCG-0.2	11.7	6.6	40.0	26.3	11.5	11.7	3.9	27.8	59.1	3.9	9.2

Reaction conditions: P = 4 MPa, $H_2/CO/N_2$ = 8/4/1, T = 290 °C, GHSV = 6000 mL $g_{cat}^{-1}\cdot h^{-1}$. [a] X_{co} is CO conversion. [b] S_{co_2} is the selectivity to CO_2. [c] S_{ROH} is the selectivity to the total alcohols. i in C_i is number of carbon atoms for the carbon-contained products. C_{4+} represents the carbon-contained products with 4 or more carbon atoms.

As for LCG, seen from the above TEM and XRPD results, the composition after reduction is the same with that after reaction, and all are Co/$La_4Ga_2O_9$. In addition, the smaller BET surface area for LCG makes the Co nanoparticle severely sintered and unevenly dispersed (see in Table 2), thus resulting in a poor activity. At the same time, the larger Co particle sizes and the strong effects between Ga and La in the catalyst are also detrimental to the generation of the Co-Ga interfaces. The interfaces of Co and Ga were usually considered to be the active sites for HAS [16], while metal cobalt was the

active sites of hydrocarbon generation [14]. Therefore, the LCG catalyst has the highest hydrocarbon selectivity among all the samples.

However, as for LKCG-0.1 catalyst, the main composition after reduction is Co/K_2O-La_2O_3-$LaGaO_3$ and the main composition after reaction is Co/K_2O-La_2O_3-$La_2O_2CO_3$-$LaGaO_3$ (seen from the XRPD results). It is known from Table 4 that the catalyst with the optimal catalytic performance is LKCG-0.1. Since they have a larger specific surface area, cobalt nanoparticles are highly dispersed on the catalyst surface, which can be seen in Figure 5 and Table 2. In addition, since all the elements located in the lattice of perovskite, smaller size and uniformly dispersed cobalt nanoparticles are also conducive to generating more Co-Ga interfaces. In the process of reaction, cobalt exists in the form of Co^0. The close contact of cobalt with the Co-Ga interface at the atomic level is beneficial to the synergistic effect of the catalyst, and thus the LKCG-0.1 catalyst exhibits the best catalytic performance. In addition, the electron donating effect of K can promote the increase of the selectivity of higher alcohols [31–34].

For the LKCG-0.2 catalyst, with the increasing of K content, the catalytic activity decreased, for that the addition of K can make part of Co outside the perovskite structure, resulting in a non-uniform dispersion of Co and Ga. A relatively lower activity and selectivity is observed in Table 4.

Other catalysts with outstanding performance reported in the literature are revealed in Table 5 [17,35–38]. By comparison, the activity of LKCG-0.1 catalyst in this work is not the optimal, but it may be one of the good catalysts in general considering relatively lower reaction temperatures and higher alcohol selectivity for HAS.

Table 5. Performance of CO hydrogenation reported in the literature.

Catalysts	Temperature (°C)	H_2/CO [a]	Pressure (MPa)	GHSV (h^{-1})	X_{CO} (%)	S_{ROH} (%)	EtOH (%) [b]	$C_{2+}OH$ [c] (%)	Ref.
$LaCo_{0.7}Cu_{0.3}O_3$	300	2	6.9	15000	16.0	38.1	37.0	53.8	[37]
Cu-Co/La_2O_3-SiO_2	330	2	3	3900	32.1	39.5	47.5	66.1	[36]
Cu-Co/Al_2O_3	250	2	2	1800	23.2	23.3	-	79.3	[35]
Co_3Cu_1-11%CNT	300	2	5	7000	26.5	49.8	-	69.9	[38]
15Co-2.5Ga/AC	220	2	3	4000	13.1	30.3	-	24.5	[17]
LKCG-0.1	290	2	4	6000	13.2	43.6	58.1	69.1	This work

[a] Molar ratio. [b] The ethanol's mass fraction in all alcohols. [c] The mass fraction of the higher alcohols in all alcohols.

Figure 7 presents the carbon monoxide hydrogenation performance for 200-h stability tests of LKCG-0.1 catalyst. Seen from Figure 7, the alcohol's selectivity and CO conversion still maintained stability, which are remained at 19.8% and 41.8%, and the higher alcohols in all alcohols stabilized at 72.8%. The outstanding stability can be owned to the uniform dispersion of the active sites, stable catalyst structure, good sintering resistance, and more Co-Ga interfaces.

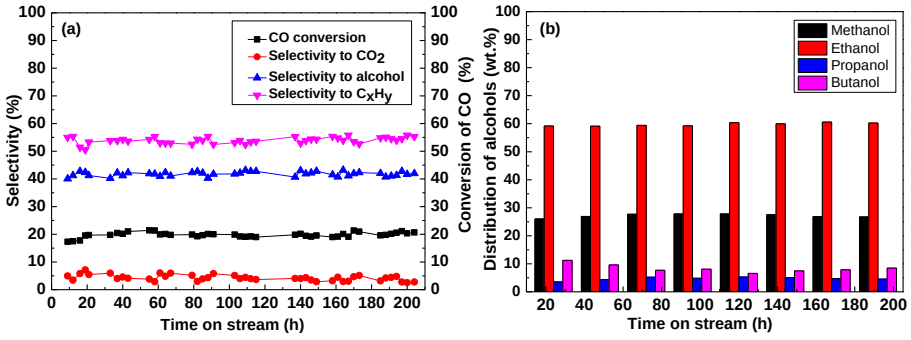

Figure 7. (**a**) Stability performance and (**b**) alcohols distributions (seen from the illustration) of the LKCG-0.1 catalyst after 200 h reaction at T = 290 °C, P = 4 MPa, GHSV = 6000 mL g_{cat}^{-1} h^{-1}, and $H_2/CO/N_2$ = 8/4/1.

2.7. Thermo-Gravimetry (TG)

Figure 8 exhibited the TG curves of the reduced and used LCG and LKCG-x (x = 0.1 and 0.2) catalysts and the corresponding differential thermal gravity (DTG) curves of the used catalysts. In Figure 8, the weight of the three reduced samples increases in the temperature range of 200–320 °C, which is attributed to the oxidation of metal cobalt nanoparticles on the surface of the catalysts. Therefore, the TG profiles of the catalysts after reduction was severed as a datum to explore the carbon deposition amount of the catalysts after reaction. In Figure 8b, two exothermic peaks can be seen for all the samples. The peak located at 300–600 °C can be attributed to amorphous carbon; while the other peak at 600–800 °C to the graphitized carbon [39]. Seen from Figure 8b, the incorporation of K can significantly reduce the total amount and formation rate of amorphous carbon, and for that K can modulate the composition of the catalysts and produce amount of La_2O_3, which is beneficial to the coke elimination.

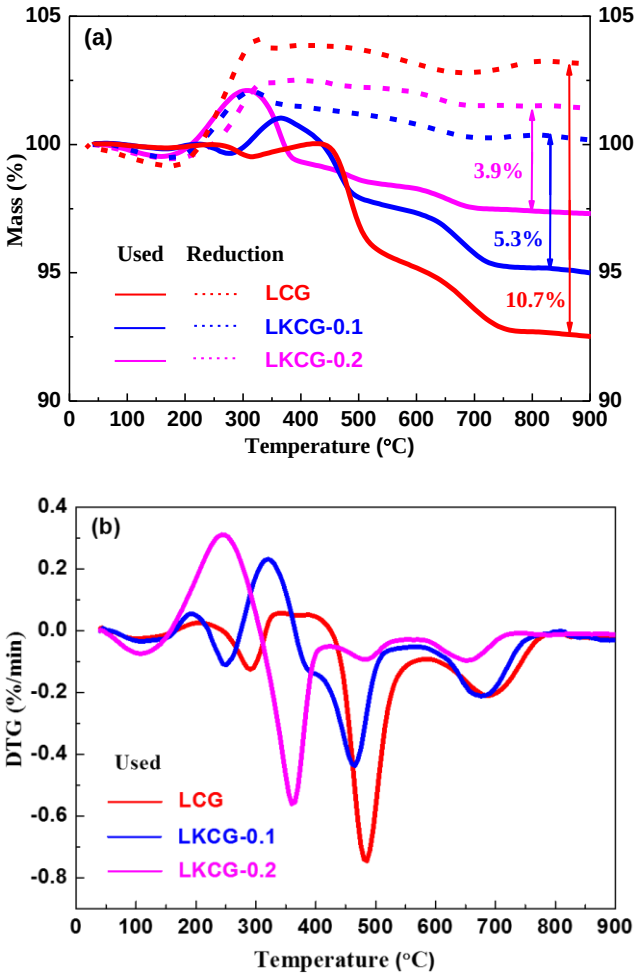

Figure 8. (**a**) Thermo-gravimetric (TG) curves of the reduced and used catalysts and (**b**) differential thermal gravity (DTG) curves of the used catalysts.

Seen from the Figure 8, the carbon deposition amounts of LKCG-0.2, LKCG-0.1 and LCG after reaction are 3.9%, 5.3% and 10.7%, respectively; in other words, the addition of K significantly relieves the formation of carbon deposition.

For LKCG-x (x = 0.1 and 0.2) catalysts, the containing carbon content of the two catalysts is almost similar. Compared to LCG catalyst, the adding of K leads to a decrease of carbon deposition. According to the above XRPD and XPS results for the reduced LKCG-x catalysts, the doping of K can modulate the composition of La-Ga-O, generating more La_2O_3, which has a better carbon-depleting effect.

Herein, the formula of $CO_2 + La_2O_3 \rightarrow La_2O_2CO_3 \xrightarrow{C} 2CO + La_2O_3$ is used to illustrate the process of removing carbon deposits during the reaction, indicating that more La_2O_3 favors the anti-carbon effect of catalysts [19,40–42]. In addition, seen from the used XRPD pattern for LKCG-x catalysts, both La_2O_3 and $La_2O_2CO_3$ can also be detected, explaining that the above mechanism is correct. Therefore, the K-doped catalyst exhibits the best anti-carbon deposition performance.

For the LCG catalyst, seen from the used XRPD result, no La_2O_3 and $La_2O_2CO_3$ can be detected. Meanwhile, there is a strong effects between La and Ga, which is not conducive to eliminating carbon deposited, and thus the carbon content of the LCG catalyst is largest.

3. Materials and Methods

3.1. Material

Lanthanum (III) nitrate hexahydrate, citrate acid, cobalt (II) nitrate hexahydrate, potassium nitrate, and glycol were bought from Shanghai Aladdin. Gallium (III) nitrate nonahydrate was purchased from Beijing HWRK Chem. All of above materials were used without further purification.

3.2. Catalysts' Synthesis

The citrate complexation method was used to prepare the K-doping catalysts [43]. Firstly, a solution with La, K, Co, Ga nitrates and citric acid, glycol are mixed by using deionized water, in which the molar ratio of lanthanum:potassium:cobalt:gallium:citric acid:glycol is 1−x:x:0.65:0.35:2.4:0.48. Secondly, the above prepared mixed solution was continuously stirred to gel at 80 °C, and then dried overnight at 120 °C. Finally, the powder catalysts were calcined at 350 °C for 2 h and 700 °C for 5 h (with a heating speed of 2 °C min^{-1}), respectively. The obtained $La_{1-x}K_xCo_{0.65}Ga_{0.35}O_3$ were labeled as LKCG-x (x = 0.1 or 0.2, which is the content of K in perovskite).

For comparison, $LaCo_{0.65}Ga_{0.35}O_3$ without K doping was prepared according to the above method, and the sample was labeled as LCG.

3.3. Catalysts' Characterization

XRPD patterns were performed at the speed of 8 °C min^{-1} between 20° and 80° (2θ). TPR were performed between 30° and 900 °C in 5% H_2/Ar (50 mL min^{-1}) at the heating rate 10 °C min^{-1}. TEM images, the EDS line scans and the corresponding element mapping scans analysis were performed to observe the component structure of the catalysts. The N_2 physical adsorption curve were tested to calculate the BET surface areas, the pore size distributions, and the pore volumes of the catalysts. XPS profiles were used to analyze the binding energy of elements, and the binding energy (BE) of C 1s was 284.6 eV. TG was performed between 30 °C and 900 °C in air at the heating speed of 10 °C min^{-1}. H_2-TPD was used to analyze the dispersion degree and size of metal cobalt. The formula of d (Co^0) = 96/D was used to calculate the size of metal cobalt, and the dispersion of metal cobalt was conducted by using the method reported in literatures [44,45].

3.4. Catalysts' Performance

The CO hydrogenation performance of catalysts were tested in a fixed-bed reactor; 0.4 g samples and 0.4 g quartz sand in 40–60 mesh were mixed and used for the HAS reaction. Temperature, pressure and gas hourly space velocity were set to 290 °C, 4 MPa and 6000 mL·g_{cat}^{-1}·h^{-1}, respectively. The molar ratio of H_2/CO is 2/1, and the internal standard gas of reaction was N_2. Before reaction, the catalysts precursors were reduced at 750 °C and remained 3 h in pure H_2 atmosphere. A TCD detector was used for analyzing H_2, N_2, CO, CO_2, and CH_4; the hydrocarbons and alcohols were detected by

using a FID detector. The following formula is used to calculate CO conversion (X_{CO}), the selectivity to product (S_i), and the weight fraction to product (W_i):

$$X_{CO} = \frac{CO_{in} - CO_{out}}{CO_{in}} \times 100\% \quad (1)$$

$$S_i = \frac{nC_i}{\sum nC_i} \times 100\% \quad (2)$$

$$W_i = \frac{m_i}{\sum m_i} \times 100\% \quad (3)$$

CO_{in} and CO_{out} represent the moles fraction of CO in the inlet and outlet gases, respectively; n is the carbon atoms number, and C_i is the mole fractions of carbon-containing products. m_i is the weight of alcohol.

4. Conclusions

$La_{0.9}K_{0.1}Co_{0.65}Ga_{0.35}O_3$ with a perovskite structure was prepared by using the citrate complexation method. Due to all the components being derived from the perovskite structure, after reduction Co is firmly confined to the K-modified La-Ga-O composite oxides, resulting in excellent anti-sintering performance. The addition of K can modulate the composition of La-Ga-O, forming more La_2O_3, favoring the improvement of anti-carbon deposition performance. In addition, the addition of K also increases the dispersion of cobalt, which can generate a greater Co-Ga interface. What is more important is that the doping of K can provide more electron donors for metallic Co, which enhances the selectivity to higher alcohols. Therefore, the catalysts show excellent catalytic activity, high selectivity to higher alcohol, and outstanding stability for the HAS.

Author Contributions: Formal analysis, S.G.; Investigation, S.G., T.H. and Z.Z.; Project administration, G.L. and Y.L.; Resources, Y.L.; Supervision, G.L. and Y.L.; Visualization, S.G.; Writing–original draft, S.G.; Writing–review and editing, G.L.

Funding: This research was funded by National Natural Science Foundation of China [Nos. 21576192 and 21872101] and The APC was funded by Key Science and Technology Program of Henan Province [Nos. 182102210432].

Acknowledgments: The financial support of this work by the National Natural Science Foundation of China (NSFC) (Nos. 21576192 and 21872101), Key Science and Technology Program of Henan Province (Nos. 182102210432) are gratefully acknowledged.

Conflicts of Interest: The authors declare no conflict of interest.

References

1. Baker, J.E.; Burch, R.; Golunski, S.E. Synthesis of higher alcohols over copper/cobalt catalysts. Influence of preparative procedures on the activity and selectivity of Cu/Co/Zn/Al mixed oxide catalysts. *Appl. Catal.* **1989**, *53*, 279–297. [CrossRef]
2. Surisetty, V.R.; Dalai, A.K.; Kozinski, J. Alcohols as alternative fuels: An overview. *Appl. Catal. A-Gen.* **2011**, *404*, 1–11. [CrossRef]
3. Atsumi, S.; Hanai, T.; Liao, J.C. Non-fermentative pathways for synthesis of branched-chain higher alcohols as biofuels. *Nature* **2008**, *451*, 86–90. [CrossRef] [PubMed]
4. Herman, R.G. Advances in catalytic synthesis and utilization of higher alcohols. *Catal. Today* **2000**, *55*, 233–245. [CrossRef]
5. Yu, S.; Tao, J. Economic, energy and environmental evaluations of biomass-based fuel ethanol projects based on life cycle assessment and simulation. *Appl. Energy* **2009**, *86*, S178–S188. [CrossRef]
6. Subramanian, N.D.; Gao, J.; Mo, X.; Goodwin, J.G., Jr.; Torres, W.; Spivey, J.J. La and/or V oxide promoted Rh/SiO_2 catalysts: Effect of temperature, H_2/CO ratio, space velocity, and pressure on ethanol selectivity from syngas. *J. Catal.* **2010**, *272*, 204–209. [CrossRef]

7. Abdelsayed, V.; Shekhawat, D.; Poston, J.A.; Spivey, J.J. Synthesis, characterization, and catalytic activity of Rh-based lanthanum zirconate pyrochlores for higher alcohol synthesis. *Catal. Today* **2013**, *207*, 65–73. [CrossRef]
8. Surisetty, V.; Eswaramoorthi, I.; Dalai, A. Comparative study of higher alcohols synthesis over alumina and activated carbon-supported alkali-modified MoS_2 catalysts promoted with group VIII metals. *Fuel* **2012**, *96*, 77–84. [CrossRef]
9. Christensen, J.M.; Duchstein, L.D.L.; Wagner, J.B.; Jensen, P.A.; Temel, B.; Jensen, A.D. Catalytic Conversion of Syngas into Higher Alcohols over Carbide Catalysts. *Ind. Eng. Chem. Res.* **2012**, *51*, 4161–4172. [CrossRef]
10. Bai, Y.; He, D.; Ge, S.; Liu, H.; Liu, J.; Huang, W. Influences of preparation methods of ZrO_2 support and treatment conditions of Cu/ZrO_2 catalysts on synthesis of methanol via CO hydrogenation. *Catal. Today* **2010**, *149*, 111–116. [CrossRef]
11. Nunan, J.G.; Bogdan, C.E.; Klier, K.; Smith, K.J.; Young, C.W.; Herman, R.G. Methanol and C_2 oxygenate synthesis over cesium doped CuZnO and $Cu/ZnO/Al_2O_3$ catalysts: A study of selectivity and ^{13}C incorporation patterns. *J. Catal.* **1988**, *113*, 410–433. [CrossRef]
12. Fang, K.; Li, D.; Lin, M.; Xiang, M.; Wei, W.; Sun, Y. A short review of heterogeneous catalytic process for mixed alcohols synthesis via syngas. *Catal. Today* **2009**, *147*, 133–138. [CrossRef]
13. Xiao, K.; Bao, Z.; Qi, X.; Wang, X.; Zhong, L.; Fang, K.; Lin, M.; Sun, Y. Structural evolution of CuFe bimetallic nanoparticles for higher alcohol synthesis. *J. Mol. Catal. A-Chem.* **2013**, *378*, 319–325. [CrossRef]
14. Xiao, K.; Qi, X.; Bao, Z.; Wang, X.; Zhong, L.; Fang, K.; Lin, M.; Sun, Y. CuFe, CuCo and CuNi nanoparticles as catalysts for higher alcohol synthesis from syngas: A comparative study. *Catal. Sci. Technol.* **2013**, *3*, 1591–1602. [CrossRef]
15. An, Z.; Ning, X.; He, J. Ga-promoted CO insertion and C–C coupling on Co catalysts for the synthesis of ethanol and higher alcohols from syngas. *J. Catal.* **2017**, *356*, 157–164. [CrossRef]
16. Ning, X.; An, Z.; He, J. Remarkably efficient CoGa catalyst with uniformly dispersed and trapped structure for ethanol and higher alcohol synthesis from syngas. *J. Catal.* **2016**, *340*, 236–247. [CrossRef]
17. Gao, S.; Li, X.; Li, Y.; Yu, H.; Zhang, F.; Sun, Y.; Fang, H.; Zhang, X.; Liang, X.; Yuan, Y. Effects of gallium as an additive on activated carbon-supported cobalt catalysts for the synthesis of higher alcohols from syngas. *Fuel* **2018**, *230*, 194–201. [CrossRef]
18. Zhao, L.; Wei, Y.; Huang, Y.; Liu, Y. $La_{1-x}K_xFe_{0.7}Ni_{0.3}O_3$ catalyst for ethanol steam reforming—The effect of K-doping. *Catal. Today* **2016**, *259*, 430–437. [CrossRef]
19. Morales, M.; Segarra, M. Steam reforming and oxidative steam reforming of ethanol over $La_{0.6}Sr_{0.4}CoO_{3-\delta}$ perovskite as catalyst precursor for hydrogen production. *Appl. Catal. A-Gen.* **2015**, *502*, 305–311. [CrossRef]
20. Lee, M.; Jung, W. Hydrothermal Synthesis of $LaCO_3OH$ and Ln^{3+}-doped $LaCO_3OH$ Powders under Ambient Pressure and Their Transformation to $La_2O_2CO_3$ and La_2O_3. *Bull. Korean Chem. Soc.* **2013**, *34*, 3609–3614. [CrossRef]
21. Kathiraser, Y.; Wang, Z.; Yang, N.-T.; Zahid, S.; Kawi, S. Oxygen permeation and stability study of $La_{0.6}Sr_{0.4}Co_{0.8}Ga_{0.2}O_{3-\delta}$ (LSCG) hollow fiber membrane with exposure to CO_2, CH_4 and He. *J. Membr. Sci.* **2013**, *427*, 240–249. [CrossRef]
22. Levasseur, B.; Kaliaguine, S. Methanol oxidation on $LaBO_3$ (B=Co, Mn, Fe) perovskite-type catalysts prepared by reactive grinding. *Appl. Catal. A-Gen.* **2008**, *343*, 29–38. [CrossRef]
23. Royer, S.; Bérubé, F.; Kaliaguine, S. Effect of the synthesis conditions on the redox and catalytic properties in oxidation reactions of $LaCo_{1-x}Fe_xO_3$. *Appl. Catal. A-Gen.* **2005**, *282*, 273–284. [CrossRef]
24. Fang, Y.; Liu, Y.; Deng, W.; Liu, J. Cu-Co bi-metal catalyst prepared by perovskite $CuO/LaCoO_3$ used for higher alcohol synthesis from syngas. *J. Energy Chem.* **2014**, *23*, 527–534. [CrossRef]
25. Chagas, C.A.; Toniolo, F.S.; Magalhães, R.N.; Schmal, M. Alumina-supported $LaCoO_3$ perovskite for selective CO oxidation (SELOX). *Int. J. Hydrogen Energy* **2012**, *37*, 5022–5031. [CrossRef]
26. Song, Z.; Shi, X.; Ning, H.; Liu, G.; Zhong, H.; Liu, Y. Loading clusters composed of nanoparticles on ZrO_2 support via a perovskite-type oxide of $La_{0.95}Ce_{0.05}Co_{0.7}Cu_{0.3}O_3$ for ethanol synthesis from syngas and its structure variation with reaction time. *Appl. Surf. Sci.* **2017**, *405*, 1–12. [CrossRef]
27. Zhan, H.; Li, F.; Gao, P.; Zhao, N.; Xiao, F.; Wei, W.; Zhong, L.; Sun, Y. Methanol synthesis from CO_2 hydrogenation over La–M–Cu–Zn–O (M = Y, Ce, Mg, Zr) catalysts derived from perovskite-type precursors. *J. Power Sources* **2014**, *251*, 113–121. [CrossRef]

28. Jena, H.; Govindan, K.; Kutty, T. Novel wet chemical synthesis and ionic transport properties of $LaGaO_3$ and selected doped compositions at elevated temperatures. *Mater. Sci. Eng. B* **2004**, *113*, 30–41. [CrossRef]
29. Majima, T.; Kono, E.; Ogo, S.; Sekine, Y. Pre-reduction and K loading effects on noble metal free Co-system catalyst for water gas shift reaction. *Appl. Catal. A-Gen.* **2016**, *523*, 92–96. [CrossRef]
30. Yang, Q.; Cao, A.; Kang, N.; An, K.; Liu, Z.; Liu, Y. A new catalyst of Co/La_2O_3-doped $La_4Ga_2O_9$ for direct ethanol synthesis from syngas. *Fuel Process. Technol.* **2018**, *179*, 42–52. [CrossRef]
31. Boz, I. Higher alcohol synthesis over a K-promoted Co_2O_3-CuO-ZnO-Al_2O_3. *Catal. Lett.* **2003**, *87*, 187–194. [CrossRef]
32. Courty, P.; Durand, D.; Freund, E.; Sugeer, A. C1-C6 alcohols from synthesis gas on copper-cobalt catalysts. *J. Mol. Catal.* **1982**, *17*, 241–254. [CrossRef]
33. Sheffer, G.R.; Jacobson, R.A.; King, T.S. Chemical nature of alkali-promoted copper-cobalt-chromium oxide higher alcohol catalysts. *J. Catal.* **1989**, *116*, 95–107. [CrossRef]
34. Sheffer, G.R.; King, T.S. Effect of preparation parameters on the catalytic nature of potassium promoted CuCoCr higher alcohol catalysts. *Appl. Catal.* **1988**, *44*, 153–164. [CrossRef]
35. Wang, J.; Chernavskii, P.A.; Khodakov, A.Y.; Wang, Y. Structure and catalytic performance of alumina-supported copper–cobalt catalysts for carbon monoxide hydrogenation. *J. Catal.* **2012**, *286*, 51–61. [CrossRef]
36. Liu, G.; Niu, T.; Pan, D.; Liu, F.; Liu, Y. Preparation of bimetal Cu–Co nanoparticles supported on meso–macroporous SiO_2 and their application to higher alcohols synthesis from syngas. *Appl. Catal. A-Gen.* **2014**, *483*, 10–18. [CrossRef]
37. Tien-Thao, N.; Zahedi-Niaki, M.H.; Alamdari, H.; Kaliaguine, S. Conversion of syngas to higher alcohols over nanosized $LaCo_{0.7}Cu_{0.3}O_3$ perovskite precursors. *Appl. Catal. A-Gen.* **2007**, *326*, 152–163. [CrossRef]
38. Dong, X.; Liang, X.; Li, H.; Lin, G.; Zhang, P.; Zhan, H. Preparation and characterization of carbon nanotube-promoted Co–Cu catalyst for higher alcohol synthesis from syngas. *Catal. Today* **2009**, *147*, 158–165. [CrossRef]
39. Liu, G.; Cui, J.; Luo, R.; Liu, Y.; Huang, X.; Wu, N.; Jin, X.; Chen, H.; Tang, S.; Kim, J.; et al. 2D MoS_2 grown on biomass-based hollow carbon fibers for energy storage. *Appl. Surf. Sci.* **2019**, *469*, 854–863. [CrossRef]
40. Tsipouriari, V.A.; Verykios, X.E. Carbon and Oxygen Reaction Pathways of CO_2 Reforming of Methane over Ni-La_2O_3 and Ni-Al_2O_3 Catalysts Studied by Isotopic Tracing Techniques. *J. Catal.* **1999**, *187*, 85–94. [CrossRef]
41. Verykios, X.E. Catalytic dry reforming of natural gas for the production of chemicals and hydrogen. *Int. J. Hydrogen Energy* **2003**, *106*, 1045–1063. [CrossRef]
42. Li, S.; Tang, H.; Gong, D.; Ma, Z.; Liu, Y. Loading Ni/La_2O_3 on SiO_2 for CO methanation from syngas. *Catal. Today* **2017**, *297*, 298–307. [CrossRef]
43. Liu, G.; Geng, Y.; Pan, D.; Zhang, Y.; Niu, T.; Liu, Y. Bi-metal Cu–Co from $LaCo_{1-x}Cu_xO_3$ perovskite supported on zirconia for the synthesis of higher alcohols. *Fuel Process. Technol.* **2014**, *128*, 289–296. [CrossRef]
44. Liu, J.; Li, C.; Wang, F.; He, S.; Chen, H.; Zhao, Y.; Wei, M.; Evans, D.G.; Duan, X. Enhanced low-temperature activity of CO_2 methanation over highly-dispersed Ni/TiO_2 catalyst. *Catal. Sci. Technol.* **2013**, *3*, 2627–2633. [CrossRef]
45. Guo, J.; Hou, Z.; Gao, J.; Zheng, X. Production of Syngas via Partial Oxidation and CO_2 Reforming of Coke Oven Gas over a Ni Catalyst. *Energy Fuels* **2008**, *22*, 1444–1448. [CrossRef]